Dependence of radiated sound frequency on vortex core dynamics in multiple vortex interactions

Z. C. Zheng and W. Li
zzheng@ksu.edu
Department of Mechanical and Nuclear Engineering
Kansas State University, Manhattan
Kansas, USA

ABSTRACT

With both theoretical analysis and measurement data, it has been identified previously that there exists a robust sound emission from a pair of counter-rotating aircraft wake vortices at the frequency of unsteady vortex core rotation. In a vortex system with multiple vortices, the sound emission frequency can be subjected to change because of interactions among the vortices. The behaviour of the influence, indicated by the ratio between the core size and the distance of the vortices and the underlining vortex core dynamic mechanisms, is investigated in this study. A vortex particle method is used to simulate the vortex core dynamics in two-dimensional, inviscid and incompressible flow. The flow field, in the form of vorticity, is employed as the source in the far-field acoustic calculation using a vortex sound formula. Cases of co-rotating vortices and a multiple-vortex system composed of two counter-rotating vortex pairs are studied for applications to aircraft wake vortex sound. The study shows, without vortex merging, individual frequencies can be clearly identified that are due each to core rotation (self induction) and co-rotating motion of a vortex centre around the other (mutual induction). The ratio of the core size and the distance between vortices does not seem to significantly influence the frequency of vortex core rotation. With vortex merging, a single frequency due to the merged vortex core is generated.

1.0 INTRODUCTION

A recent scheme for actively monitoring wake vortices has emerged by passively tracking the acoustic emissions from wake vortices[1-2], in addition to previous efforts in developing engineering prediction models for the wake vortex behaviour in response to weather conditions in the lower atmosphere[3-8]. It has been identified that vorticity in a vortex core directly relates to the frequency of a significant sound peak from an aircraft wake vortex pair where each of the vortices is modeled as an elliptic core Kirchhoff vortex. This sound source is resulted from an uneven distribution of vorticity impulse about the vortex centre in an elliptic core. When an aircraft vortex wake is represented by such a vortex pair, the vortex core size is very small in comparison with the distance between the vortices. In this case, the peak frequency remains the same as that of a single Kirchhoff vortex, equal to $\Omega/4\pi$ where Ω is the uniform vorticity in the Kirchhoff vortex core[9]. In a vortex system with multiple vortices, the peak frequencies can shift due to different straining field imposed on the vortex cores. From theoretical deduction, Tang and Ko[10-11] showed that in any vortex system, the basic sound generation mechanisms can be attributed to the vortex core deformation and the vorticity centroid dynamics. Between the two mechanisms, the vorticity centroid motion produces sound at a lower frequency, and the vortex core deformation produces sound at a higher frequency. By using the method of contour dynamics as the numerical simulation tool[12,13], they found that the frequency of the high-frequency oscillation, which is

Paper No. 3309. Manuscript received 20 June 2008, revised 14 November 2008, accepted 29 January 2009.

associated to the unsteady core deformation, is proportional to the vorticity of the vortex. It is expected that when the effect of straining from other vortices becomes insignificant, this frequency approaches to the above-mentioned sound frequency of a single Kirchhoff vortex, as shown in Ref. 1.

In a vortex system with multiple vortices such as a complicated aircraft vortex wake, this Kirchhoff vortex frequency is subjected to change because of interactions among multiple vortices. An analogy (but with totally different physical mechanisms) is similar to that between the Crow instability[14] for a single vortex pair and the Crouch instability[15] for multiple vortex pairs. Particularly, when two vortices are close to each other, the frequency may change significantly, with the extreme case of coalescence of two vortices. Although it is indicated that the ratio between the core size and the distance of the vortices influences the frequency of the sound due to vortex core dynamics[11], the behaviour of the influence and the underlined mechanisms have not been fully investigated.

Several numerical methods have been developed to simulate vortex merging[16,17]. For the purpose of investigating the related acoustic frequencies, a vortex particle method[18] is used here to simulate the vortex core dynamics in the two-dimensional, inviscid and incompressible flow. The flow field, in the form of vorticity, is employed as the source in the far-field acoustic calculation using a vortex sound formula[1], similar to the two-dimensional version of Mohring[19,20] and others[9,10,21-24]. This method has been used and verified in the cases of a single Kirchhoff vortex and a pair of counter-rotating vortices[1].

In the following discussions, we first look at a co-rotating vortex pair to investigate the effect of the mutual induction between the two co-rotating vortices on the frequency content of radiated sound. Then a number of different configurations of multiple-vortex systems composed of two counter-rotating vortex pairs are studied. These configurations are selected for the purpose of applying the present results to the study of aircraft wake sound.

The objective of the paper is two-fold: (a) to conduct a systematic study of frequency change due to vortex merging in a multiple-vortex system, which fills a void in the data base of the current knowledge of sound generation due to vortex merging; and (b) to apply the theoretical study to a more practical case of aircraft wake vortices. Under the cruise condition, aircraft wake vortices roll up into a pair of counter-rotating vortices quickly in the far field. However, depending on aircraft configurations, such as taking off and landing when the slat or the flap is fully deployed and the aircraft is close to the ground, the multiple vortex system can be a substantial part of the wake. The present study is then able to provide an indicative of when and where the multiple vortex system becomes a vortex pair by tracking the frequency change as described later in the paper.

2.0 COMPUTATIONAL FORMULATION

2.1 Flow-field simulation

We use characteristic parameters related to the configurations of realistic wake vortices to non-dimensionalise the flow simulation equations. Since only the relative values are of the interest in this study, the reason of this selection is merely for the purpose of easy interpretation of some of the results when a practical aircraft vortex wake is concerned.

The characteristic length, l_c, is 23·81 units of a nominal initial core radius a, which is intended to be the half span of the wake vortex pair in the far wake of an aircraft, with a to be 4·2% of the half span of the vortex pair. The reason to select a as a measure is because we also consider the cases that are not vortex pairs. The characteristic velocity, V_c, is the nominal maximum rotating speed at the outer edge of the vortex core, $a\Omega/2$. With the characteristic length and velocity, the characteristic time and frequency are consequently $47{\cdot}62/\Omega$ and $\Omega/47{\cdot}62$, respectively. If the circulation of an almost-circular Kirchhoff vortex is $\Gamma = \pi a^2\Omega$, then the characteristic frequency is $\Gamma/47{\cdot}62\pi a^2 = 11{\cdot}9\Gamma/l_c^2$.

All of the vortices in the simulation are initially specified as almost-circular Kirchhoff vortices, with the ellipse defined by the polar equation

$$r = a\,[1 + \varepsilon \mathrm{Cos}(2\theta - \Omega t/2)] \quad \ldots (1)$$

where the long axis of the ellipse is $a(1+\varepsilon)$, the short axis is $a(1-\varepsilon)$, and ε is selected as 0·05 ($\ll$1). Based on the characteristic parameters, we have a = 0·042, and Ω = 47·62. With this value of vorticity in the core, the corresponding theoretical sound frequency for a single vortex is $\Omega/4\pi$ = 3·79 . This simplified initial condition fits our current interest of looking into the frequency effect. More complicated shapes of vortices[25,26] could also be specified if the actual magnitude of the sound level was concerned.

In the vortex particle method[18], the vortex particles are distributed on a grid mesh with the grid size of $\Delta x = \Delta y = 1{\cdot}5 \times 10^{-3}$ and a particle core parameter, α, of $2\Delta x$[27]. This gives 50 vortex particles along a nominal vortex core diameter of $2a$. This fine grid solution requirement in the simulation has been established previously[1] and during the present study to ensure a proper resolution of the vorticity field in order to correctly capture the core rotational frequency. Simulation tests with lower resolution have shown that the acoustic frequency numerically shifts to lower values. The required high resolution in this problem poses difficulties in using the Eulerian type of simulation.

For the two dimensional problem, the distribution of vorticity is

$$\zeta(\mathbf{x}, t) = \sum_n \Gamma_n(t) g_\alpha(\mathbf{x} - \mathbf{x}_n(t)) \quad \ldots (2)$$

where Γ_n is the circulation of each vortex particle, initially defined as $(\Delta x)^2\Omega$ in the Kirchoff vortex model here, and g_α is a second-order particle core function[18] defined as

$$g_\alpha(\boldsymbol{x}) = \frac{1}{\pi\alpha^2}\exp(-|\boldsymbol{x}|^2/\alpha^2)\,. \quad \ldots (3)$$

In the simulation of this study, α, the vortex particle radius, is selected as $2\Delta x$ (or $2\Delta y$, since they are equal), following a particle radius requirement for convergence specified by Beale and Majda[28].

In the vortex particle method for the two-dimensional, inviscid and incompressible flow, the only time integration is to track the position of each particle with

$$\frac{\mathrm{d}\boldsymbol{x}_n}{\mathrm{d}t} = \boldsymbol{u}(\boldsymbol{x}_n, t)\,, \quad \ldots (4)$$

where, for the two-dimensional flow, $u(x_n,t)$ is related to the circulation of each vortex particle following the Biot-Savart law as

$$\boldsymbol{u}(\boldsymbol{x}_n, t) = \sum_m \Gamma_m(t)\boldsymbol{K}_\alpha(\boldsymbol{x}_n - \boldsymbol{x}_m) \times \boldsymbol{e}_3\,, \quad \ldots (5)$$

where K_α is a two-dimensional Biot-Savart kernel, defined as[18]

$$\boldsymbol{K}_\alpha(\boldsymbol{x}) = -\frac{\boldsymbol{x}}{2\pi|\boldsymbol{x}|}(1 - e^{-|\boldsymbol{x}|^2/\alpha^2})\,. \quad \ldots (6)$$

The size of time step is $\Delta t = 1{\cdot}0293 \times 10^{-2}$, which is equal to $5T/128$, where T is the oscillation period of a single Kirchhoff vortex equal to $4\pi/\Omega$. This time step is sufficiently small to resolve the frequency content related to the core vorticity.

During the simulation, re-meshing is done at each time step to maintain the convergence requirement on preserving vortex particle overlaps[28]. Once all the vortex particles are moved following Equation (4), they are re-distributed back to the original grid using a sixth-order kernel[29]

$$\tilde{\Gamma}_n = \sum_m W_\varepsilon(\tilde{\boldsymbol{x}}_n - \boldsymbol{x}_m)(\Delta x)^2\Gamma_m \quad \ldots (7)$$

where

$$W_\varepsilon = \frac{W(\boldsymbol{x}/\varepsilon)}{\sigma^2}\,, \quad \ldots (8)$$

$$W(x_1,x_2)=\frac{1}{\pi}\left(\frac{15}{8}-\frac{5x_1^2}{2}+\frac{x_1^4}{2}\right)\left(\frac{15}{8}-\frac{5x_2^2}{2}+\frac{x_2^4}{2}\right)e^{-(x_1^2+x_2^2)}, \quad \ldots (9)$$

$\sigma = 1{\cdot}7\Delta x$, and $\tilde{}$ means the value after the grid remeshing.

2.2 Far-field acoustic formulation

A far-field acoustic pressure formula is needed to attribute sound sources to near-field unsteady interactions in multiple vortices. A matched-asymptotic-expansion method[1,30,31] has been used that matches the inner region of incompressible vortex flow to the outer region of acoustic field. The extended formula[1] includes both the dipole-type and quadrupole-type noise sources, with a higher order expansion than those in the previous study[30,31]. It relates the position and circulation of near-field vortices to the far-field pressure, which provides additional convenience because the position and circulation are directly calculated in the present two-dimensional vortex particle method. The detailed derivation of equations used for the far-field acoustic pressure calculation for a discrete vortex system has been presented previously[1]. The formula used in this study is expressed as;

$$\begin{aligned}\hat{p}_o \;=\; & -\mathrm{i}\frac{M\omega}{4}H_1^{(2)}(\omega Mr)\sum_j\left\{\boldsymbol{F}\left[\frac{d(\Gamma_j x_j)}{dt}\right]\mathrm{Sin}\theta-\boldsymbol{F}\left[\frac{d(\Gamma_j y_j)}{dt}\right]\mathrm{Cos}\theta\right\}\\ & +\mathrm{i}\frac{M^2\omega^2}{16}H_2^{(2)}(\omega Mr)\sum_j\left\{-\boldsymbol{F}\left[\frac{d(\Gamma_j(x_j^2-y_j^2))}{dt}\right]\mathrm{Sin}2\theta\right.\\ & \left.+\boldsymbol{F}\left[\frac{d(2\Gamma_j x_j y_j)}{dt}\right]\mathrm{Cos}2\theta\right\}, \end{aligned} \quad \ldots (10)$$

where $\boldsymbol{F}$**[]** denotes the Fourier transform in time, ω is the angular sound frequency, r is the far-field distance, M is the Mach number, θ is the far-field directional angle, $H_1^{(2)}$ is the second kind Hankel function of order one, $H_2^{(2)}$ is the second kind Hankel function of order two, and the sub-index j represents the index of the near-field vortex particles. Note that Equation (10) is a dimensionless expression for far-field acoustic pressure in the frequency domain. The characteristic parameters used in the expression are the length of $23{\cdot}81a(=l_c)$, the maximum vortex rotating speed $a\Omega/2(=V_c)$, and the density of fluid ρ_0.

With only the quadrupole source from the vortex core, the dipole terms (related to Sinθ and Cosθ) in Equation (10) are zero. The strengths of the quadrupole terms depend on

$$Q_1=\frac{\mathrm{d}[\Gamma_j(x_j^2-y_j^2)]}{\mathrm{d}t} \quad \ldots (11)$$

and

$$Q_2=\frac{\mathrm{d}(2\Gamma_j x_j y_j)}{\mathrm{d}t}. \quad \ldots (12)$$

These expressions of the quadrupole sources are in agreement with those expressions for two-dimensional vortex systems by Mohring[19,20] and others[9,10,21-24]. The far-field location for calculating acoustic pressure in this paper is selected at a distance of ten characteristic lengths ($r = 10$) at the directional angle of $\theta = 90°$. A nominal Mach number of 0·27 is specified in the calculation, which represents the ratio between the characteristic velocity and the speed of sound, $V_c/c = a\Omega/2c$, where c is the speed of sound. The combination of the far-field formulation with the near-field vortex particle simulation has been applied to a single Kirchhoff vortex and the result has reached perfect agreement to that of the analytical acoustic pressure expression of Howe[9].

3.0 RESULTS AND DISCUSSIONS

3.1 Two identical co-rotating vortices

Cases of interactions of two identical co-rotating vortices are studied here to elucidate the effect of distance between the two vortices on the peak acoustic frequency resulting from the vortex core rotation. Depending on the distance relative to the core size, cases of merging or non-merging can be realised. The merger of two identical co-rotating vortices is sometimes termed symmetric vortex merger[32,33]. Saffman and Szeto[34] developed a criterion for the occurrence of symmetric vortex merger by looking at the ratio between the distance and the core radius, $\beta = G/a$, where G is the distance between the centre of the vortices. According to their theoretical study, the critical value of β for merger is approximately 3·3. Three different β-values are considered here, which are selected in the regime of non-merging and complete merging (or vortex coalescence), and near the critical point between merging and non-merging, respectively.

Figure 1 is for a case of non-merging, when the distance, G, between the two co-rotating vortices is 0·5, and thus $\beta = G/a = 11{\cdot}9$. Fig. 1(a) is the time histories of the source terms, Q_1 and Q_2. It shows that the two source terms are of the same amplitude with a phase shift. There are obviously two major frequency contents. These two frequencies are more clearly shown in Fig 1(b), the spectrum of the acoustic pressure magnitude. In this plot and all the subsequent spectrum plots, the time window to process the spectral data is the last 2,048 time steps in each case, when the time series data are nearly periodic. The time length of the window is thus $2{,}048\Delta t = 21{\cdot}08$.

Base on the simulation, the low frequency peak is at 0·1 and the high frequency one at 3·51. The low frequency is related to the circular motion of the vortex centres (or centroids, to be more precise) around one to another, and the high frequency is related to the core rotation with respect to each of its own vortex centre. This is because each of the frequency can be approximately estimated based on their mechanisms. The angular speed for the circular vortex centre motion, when assumed point vortices, has an analytical expression of $\Gamma/\pi G^2$. The acoustic pressure caused by that motion has a frequency, f_L, of $1/\pi$ of the angular speed[9]. This frequency can be expressed as

$$f_L=\Gamma/(\pi G)^2 \quad \ldots (13)$$

For the almost-circular Kirchhoff vortices, since $\Gamma = \pi\Omega a^2$, Equation (13) becomes

$$f_L=\frac{\Omega}{\pi\beta^2}. \quad \ldots (14)$$

With the parameters in this case, this frequency is approximately 0·1. The high frequency is close to the theoretical value of a single Kirchhoff vortex of $\Omega/4\pi = 3{\cdot}79$. A slightly lower frequency in the simulation can be due to the fact that the vortices in this case are no longer perfectly single Kirchhoff vortices.

When $G = 0{\cdot}126$, with the ratio of $\beta = G/a\Omega = 3$, it is within the theoretical merging criterion for co-rotating vortices, according to Saffman and Szeto[34]. In this case, the two vortices are so close to each other that the vortex coalescence occurs. Figure 2 contains four snap shots of vorticity contours during the vortex coalescence. Since the simulation is inviscid, the merging process depicted in Fig. 2 is mostly showing the convection process among the three-phase merging stated by Orlandi[17] that includes first diffusion, convection, and second diffusion. The merging process in Fig. 2 is also represented in the histories of the source terms in Fig. 3(a) where there is a transient period before the signal becomes periodic. Similar to Fig. 1(a), the two source terms have approximately the same behaviour

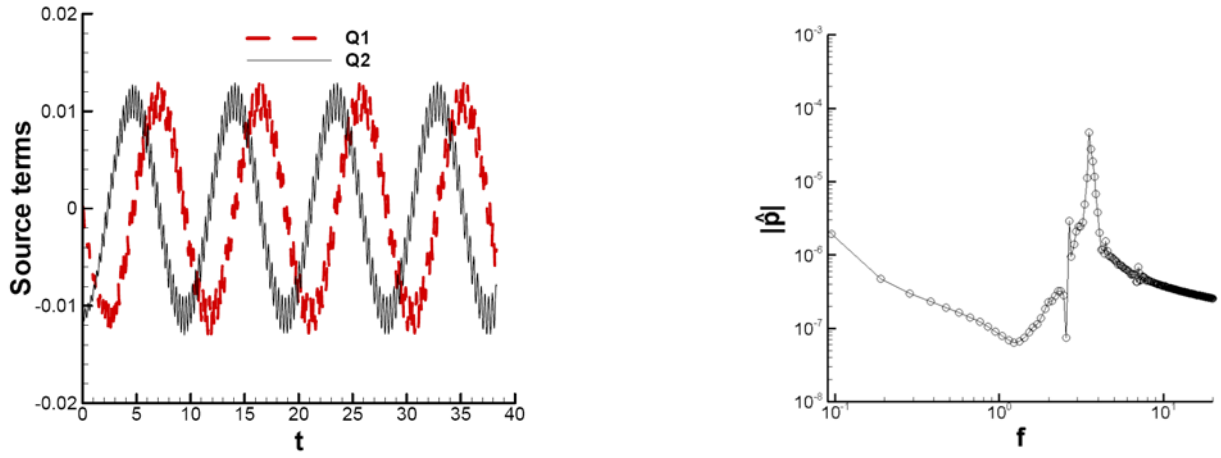

(a) (b)

Figure 1. For the case with distance G = 0·5, a = 0·042, $\beta = G/a$ = 11·9. (a) History of the quadrupole source terms in Equations (11) and (12) generated by two identical co-rotating vortices. (b) Spectrum of sound pressure magnitude in the frequency domain.

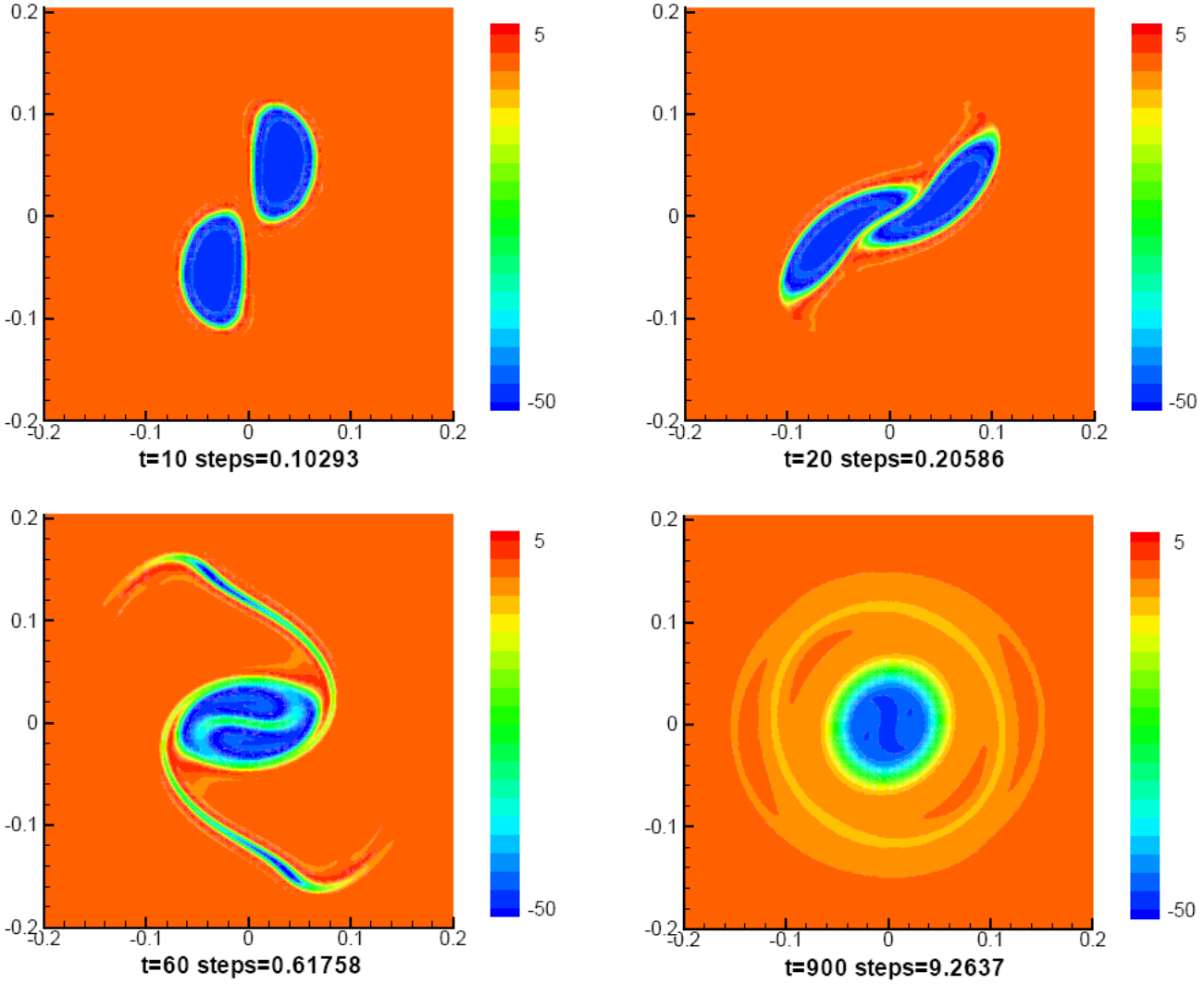

Figure 2. Snap shots of vorticity contours during the vortex merging process for the case with G = 0·126, a = 0·042, $\beta = G/a$ = 3.

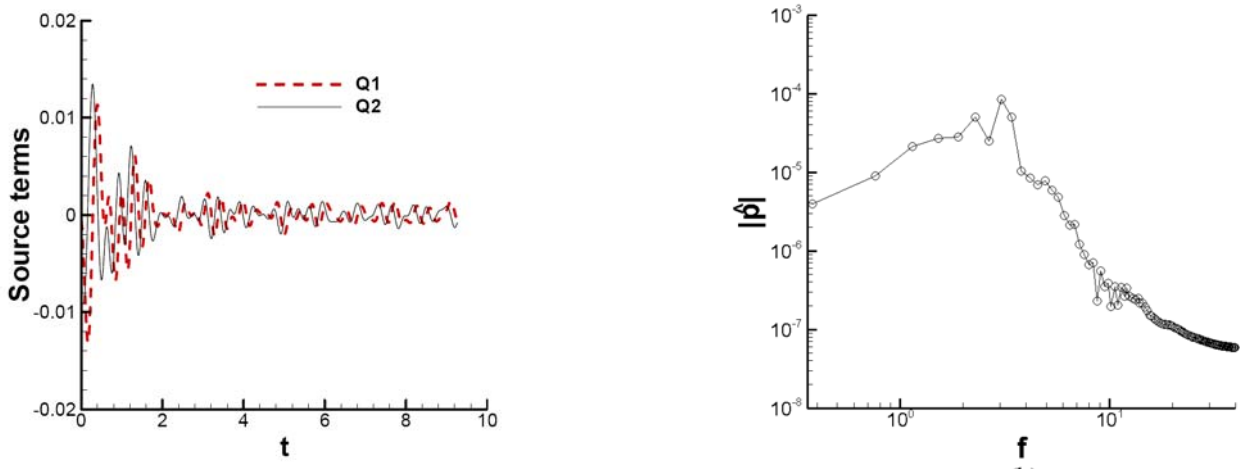

(a) (b)

Figure 3. For the same case as in Fig. 2. (a) History of the quadrupole source terms in Equations (11) and (12) generated by two identical co-rotating vortices. (b) Spectrum of sound pressure magnitude in the frequency domain.

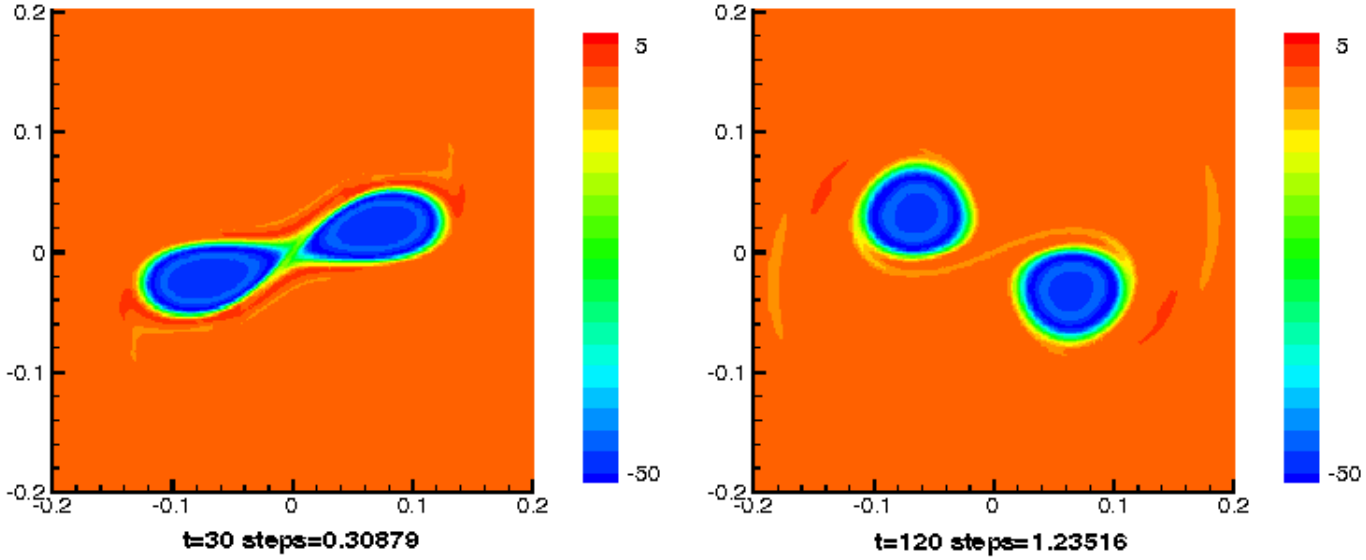

Figure 4. Snap shots of vorticity contours during the vortex merging process for the case with G = 0·147, a = 0·042, β = G/a = 3·5.

with only a phase difference. The Fourier transform in Fig. 3(b) is processed after the source terms become periodic. At this stage, there is only one significant peak at the frequency of 3·04, close to but again lower than the original single Kirchhoff vortex sound frequency. This is due to the enlarged core region of the final vortex as a result of the vortex coalescence.

A case with G = 0·147 results in β = G/a = 3·5. This β-value is a little larger than the theoretical merging distance for co-rotating vortices with uniform core vorticity with β = 3·3[34], but smaller than the merging distance for vortices with non-uniform core vorticity with β varying between 3·8 and 4·1[35]. According to our simulation, the vortex merging seems to reach a critical stage where the two vortices re-split again after touching, as shown in the snapshots of contours in Fig. 4. This phenomenon was observed by Tsuboi and Oshima[36]. As in the non-merging case, there is an angular speed for the circular vortex centre motion. For the parameters in this case, this frequency is approximately 1·24. The high frequency, due to vortex core self rotation, still exists and is approximately 3·2, a bit lower than that of a single Kirchhoff vortex of 3·79. These two frequency components are ostensible both in the time history of the quadrupole source terms, Fig. 5(a), and in the far-field pressure spectrum, Fig. 5(b).

3.2 Two vortex pairs

The same computational algorithm has been extended to simulate multiple vortex pairs. For this study, two counter-rotating vortex pairs are simulated, with the initial configuration illustrated in Fig. 6 which approximately represents an aircraft wake with multiple vortices. Because of the symmetry of the physical problem in the multiple vortex pair cases, only half of the domain needs to be

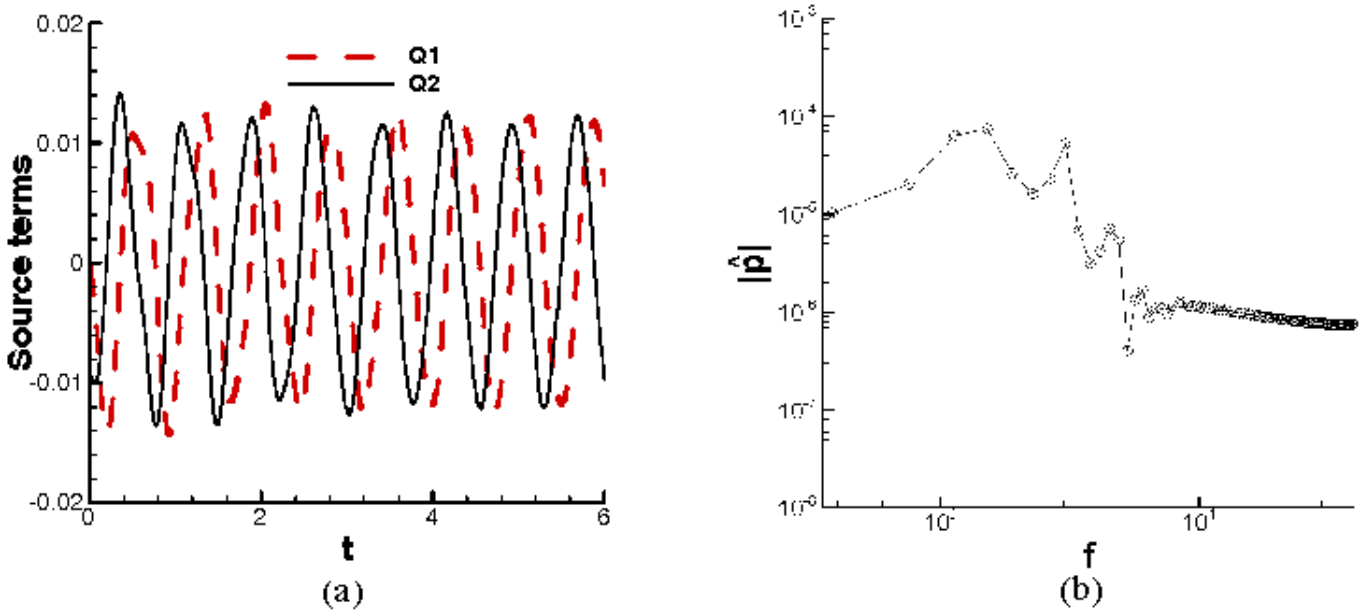

Figure 5. For the same case as in Fig. 4. (a) History of the quadrupole source terms in Equations (11) and (12) generated by two identical co-rotating vortices. (b) Spectrum of sound pressure magnitude in the frequency domain.

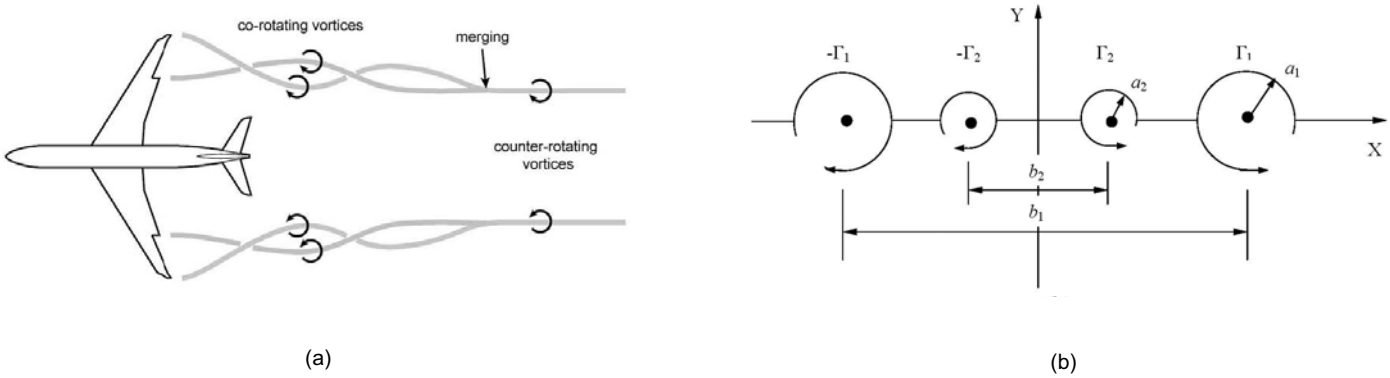

Figure 6. Illustration of (a) a typical aircraft vortex wake and (b) the initial setup of the multiple vortex pair system.

simulated and the symmetry boundary conditions are specified with respect to the centreline of the vortex system (the y-axis in Fig. 6). In the case of one inner and one outer counter-rotating vortex pairs, the Q_1 term turns out to be zero because of the vorticity symmetry in the flow field. In the following cases, the circulation of the outer vortex pair, Γ_1, is two times of that of the inner vortex pair, Γ_2.

Two non-merging cases are first presented. The vortex span of the outer vortex pair, b_1, is 2; the vortex span of the inner vortex pair, b_2, is 1. Figure 7 is for the case with $b_2/b_1 = 0{\cdot}5$, $\Omega_1 = \Omega_2 = 47{\cdot}62$, $\Gamma_1 = 2\Gamma_2$, $(a_2/a_1)^2 = 0{\cdot}5$, and $a_1 = 0{\cdot}042$. This is a case when the vorticity is the same in the two vortex pair and the circulation of the inner pair is half of that of the outer pair. Figure 8 is for the case with $b_2/b_1 = 0{\cdot}5$, $\Omega_1 = 47{\cdot}62$, $\Omega_2 = \Omega_1/2$, $\Gamma_1 = 2\Gamma_2$, $a_2/a_1 = 1$, and $a_1 = 0{\cdot}042$. This is when the vorticity and circulation of the inner pair are both half of those of the outer pair, with the core size of the two pairs remaining the same. In these cases, the distance between the two co-rotating vortices on each side is relatively large and therefore no merger occurs. It should be noted that the circulations of these two cases are the same, both with the circulation of the outer vortex pair to be twice of that of the inner vortex pair.

Figure 7(a) is plotted to compare the histories of the quadruple source term, Q_2 (since $Q_1 = 0$), using the point vortex method and the

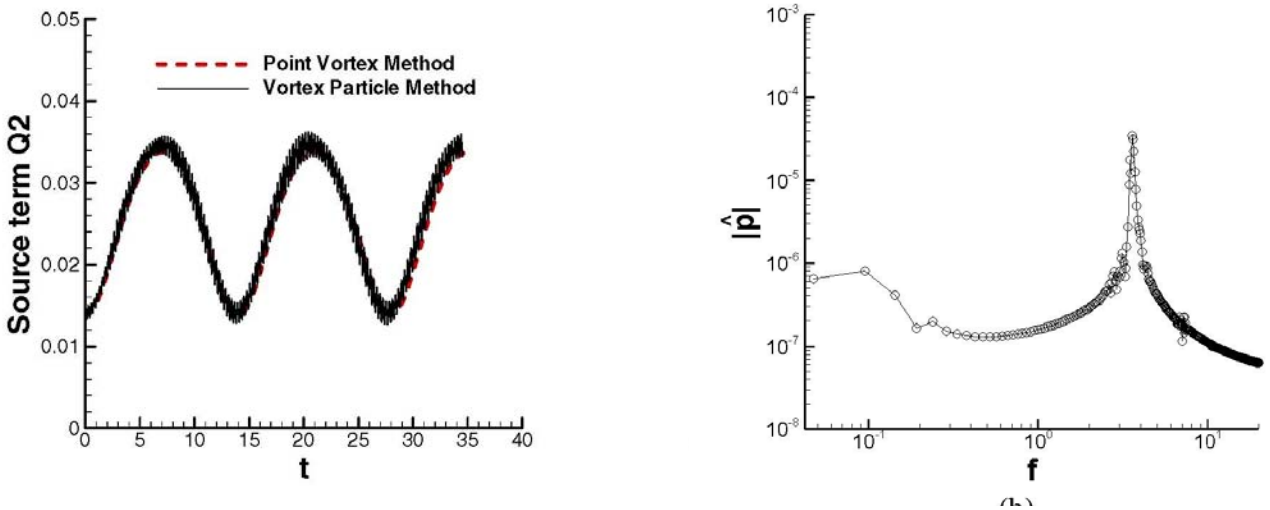

Figure 7. Two vortex pairs with the same vorticity and 1:2 ratio of the circulation without merging. (a) History of the quadrupole source term Q_2 in Equation (12). (b) Spectrum of sound pressure magnitude in the frequency domain.

vortex particle method. In the point vortex method, each vortex of the four vortices in the vortex system is represented by one point vortex. Therefore, the motion captured by the point vortex method is only that of each nominal vortex centre. Figure 7(a) shows that the history of Q_2 of the point vortex method coincides with that of the low-frequency component of the vortex particle method which is due to the centroid motion of the vortices. In the result of the vortex particle method, there is a high-frequency component caused by the vortex core vorticity, on top of the low-frequency component. In Fig. 7(b), it indicates that the low frequency peak is around 0·08, and the high frequency peak is at 3·61. The high frequency is thus again close to but lower than that of a single Kirchhoff vortex with vorticity of 47·62. As for the low frequency, for two uneven, co-rotating point vortices, the frequency for the motion of the vortex centre can be estimated by assuming point vortex for each of the vortices. The circulations of each of the vortices can be decomposed as

$$\Gamma_1 = \frac{1}{2}[(\Gamma_1+\Gamma_2)+(\Gamma_1-\Gamma_2)] \quad \ldots (15)$$

and

$$\Gamma_2 = \frac{1}{2}[(\Gamma_1+\Gamma_2)-(\Gamma_1-\Gamma_2)]. \quad \ldots (16)$$

Therefore, the two uneven vortices can be considered a superposition of a pair of co-rotating vortices with circulation of $1/2(\Gamma_1 + \Gamma_2)$ and a pair of counter-rotating vortices with circulation of $1/2(\Gamma_1 - \Gamma_2)$. While the counter-rotating vortex pair only has translational motion, the rotation of the vortex system is caused by the co-rotating vortex pair. Hence, the frequency due to the rotation of the system can be calculated following Equation (13) as

$$f_L = \frac{\frac{1}{2}(\Gamma_1+\Gamma_2)}{\pi^2(\frac{b_1-b_2}{2})^2} = \frac{2(\Gamma_1+\Gamma_2)}{\pi^2(b_1-b_2)^2}. \quad \ldots (17)$$

With the parameters in this case, the theoretical value of this frequency is also 0·08, in agreement with the simulation value.

In Fig. 8, because there are two different vorticity values in the two vortex pairs, there exist two high-frequency components, one at 3·46 and the other at 1·76, each corresponding respectively to the two vorticity values of 47·62 and 23·81 in the two pairs. The low frequency component remains around 0·08, the same as in the case in Fig. 7. This is because this frequency can also be estimated using Equation (17), and the circulations and distances in the vortex system in the case of Fig. 8 are the same as those in the case of Fig. 7.

We then present two cases with vortex merger at each side of the two-vortex-pair system that eventually becomes a one-vortex-pair system after merging. The initial vorticity, separation distance b_1, and core sizes are the same as the two non-merging cases in Figs 7 and 8, except that the distance ratio of b_2/b_1 varies to create merging.

The first case is similar to the case in Fig. 8; that is, the two vortex pairs have a 1:2 ratio in both vorticity and circulation. Therefore the core sizes of all the vortices are the same, with $a_1 = a_2 = 0{\cdot}042$ and $\Omega_1 = 47{\cdot}62 = 2\Omega_2$. The distance ratio, b_2/b_1, is specified as 0·874, resulting in $\beta = 3$ for the two co-rotating vortices at the same side of the vortex pair system. This β value, as tested previously in Section 3.1, leads to a complete vortex merger for two identical vortices. Although here the two vortices, each from a different vortex pair, have different strengths, they have the same core size and this β value still leads to a complete merger. Figure 9 is the source term history and the spectrum of the far-field pressure. The vortex merging stage shows in the early transient period of the time history. The spectrum in Fig. 9(b) is processed after the transient period. It can be seen that there is one peak at frequency of 3·42, close to the frequency produced by the higher vorticity value (of 47·62) between the two vortices. Another frequency, supposedly corresponding to the lower vorticity value (of 23·81) of one of the vortices, seems to disappear.

The second case is similar to the case in Fig. 7; that is, the two vortex pairs have a 1:2 ratio in circulation ($\Gamma_1 = 2\Gamma_2$), but the vorticity level is the same in the two ($\Omega_1 = \Omega_2 = 47{\cdot}62$). Therefore the core sizes follow a ratio of $(a_2/a_1)^2 = 0{\cdot}5$. Since the core sizes are different for the co-rotating vortices at one of the vortex pair system, an average core size is used as a nominal core size to determine the β value. In order to create vortex merger, we keep the β value approximately equal to 3, and therefore the distance ratio is changed to $b_2/b_1 = 0{\cdot}898$ accordingly. Figure 10 is the source term history and

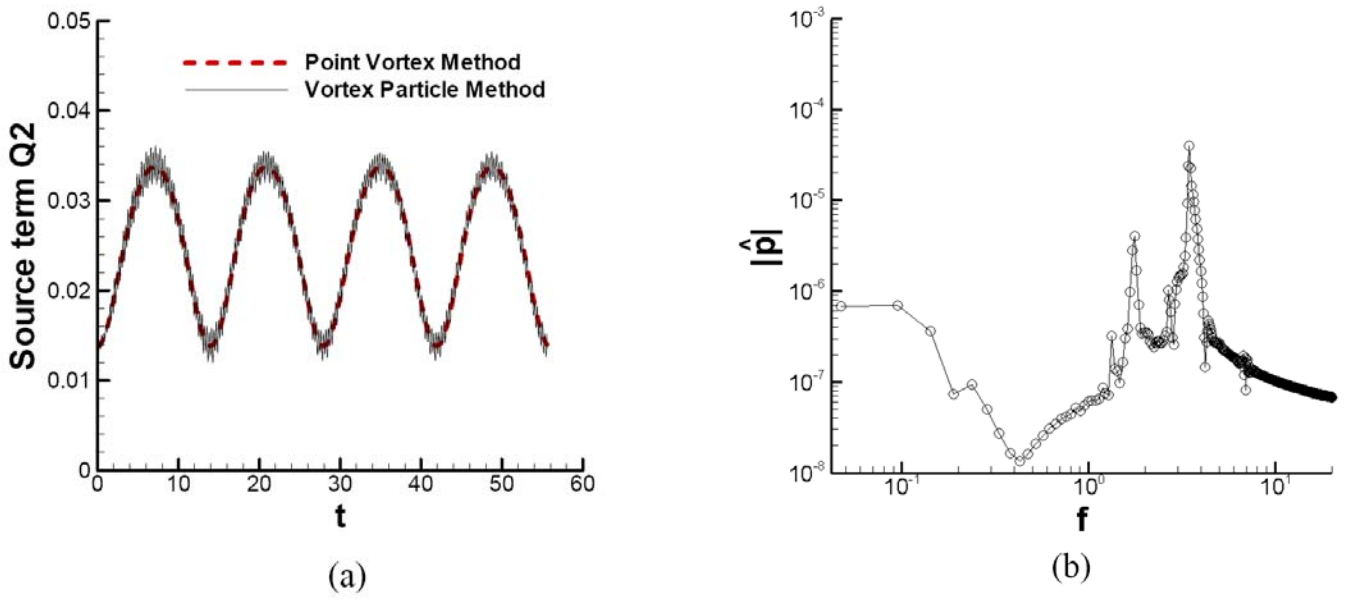

Figure 8. Two vortex pairs with 1:2 ratio in both the vorticity and circulation without merging. (a) History of the quadrupole source term Q_2 in Equation (12). (b) Spectrum of sound pressure magnitude in the frequency domain.

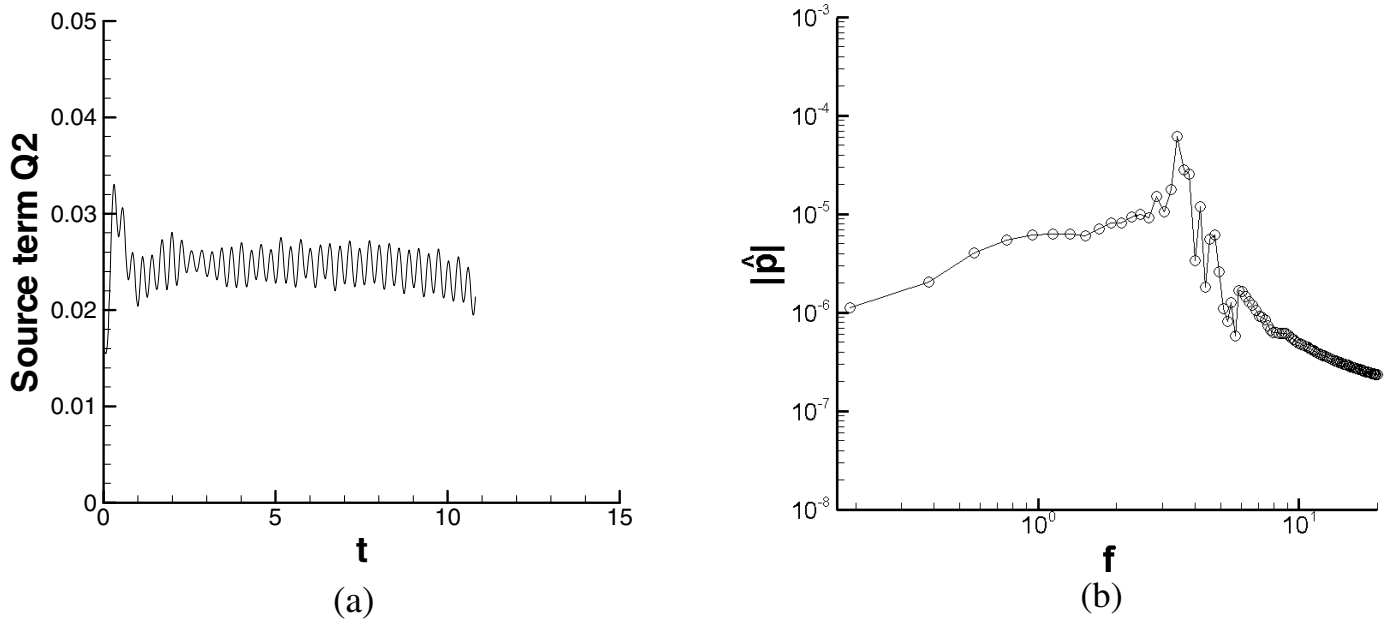

Figure 9. Two vortex pairs with 1:2 ratio in both the vorticity and circulation with merging. (a) History of the quadrupole source term Q_2 in Equation (12). (b) Spectrum of sound pressure magnitude in the frequency domain.

the spectrum of the far-field pressure for this case. Again, the spectrum is processed after the transient period of the time history. It can be seen that there is a peak at frequency of 3·23, lower than the original Kirchhoff core frequency.

The phenomena observed in Figs 9 and 10 can be explained by the contour plots in Fig. 11 that are on one side of the vortex pairs (the other side is a mirror-image of the y-axis) after merging of the two cases represented by Figs 9 and 10. Figure 11(a) is for the case of same core size, which is the case of Fig. 9; and Fig. 11(b) is for the case of same vorticity, which is the case of Fig. 10. Figure 11(a) shows that after merging, there is only one discernable high vorticity level, although before merging there are two different vorticity values in each of the vortex. The weaker vortex with lower vorticity is distorted during merging and becomes a layer wrapping around the stronger vortex that has a higher vorticity. The distortion and wrapping processes during the interactions between two unequal vortices were also observable in experiments[37]. The dominant centrifugal effect of the stronger vortex eventually tightens most of the vorticity into its core spinning at a rotational speed that is higher than the original lower vorticity. Therefore there is only one peak frequency in Fig. 9 that is related to one vorticity value. Furthermore, the tightening of the core results in a relatively smaller

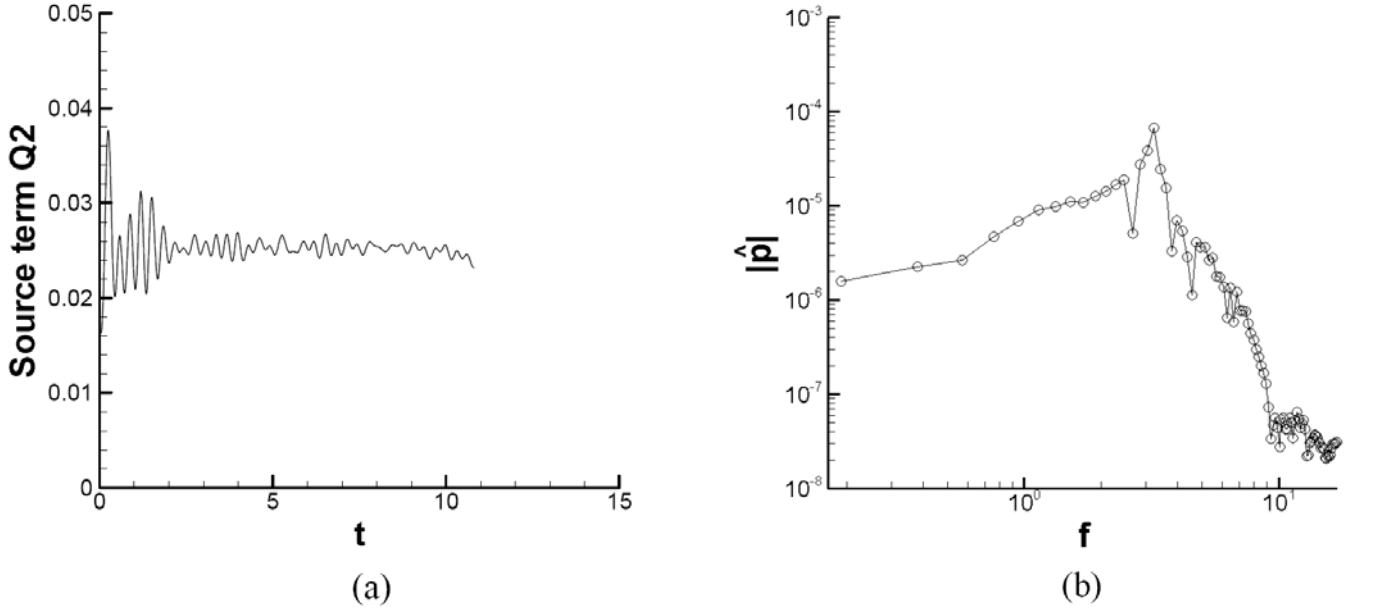

Figure 10. Two vortex pairs with the same vorticity and 1:2 ratio in circulation, with merging. (a) History of the quadrupole source term Q_2 in Equation (12) (b) Spectrum of sound pressure magnitude in the frequency domain.

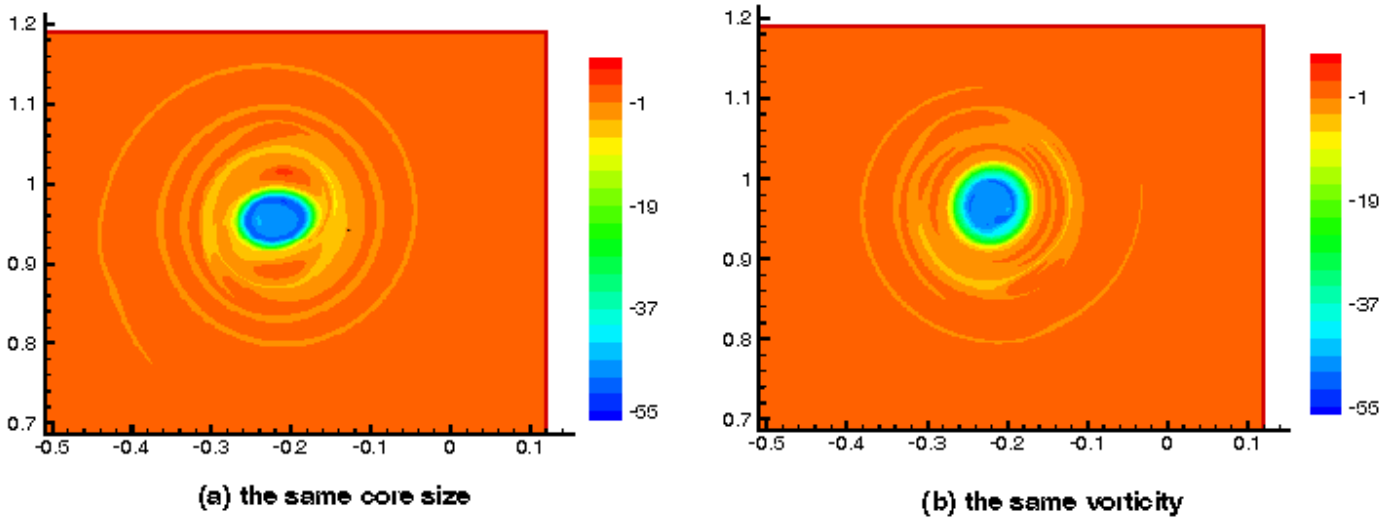

Figure 11. Vorticity contours after merging for the cases of co-rotating vortex merger in a two-vortex-pair system. (a) Same core size as in Fig. 9. (b) Same vorticity as in Fig. 10.

core in the same core size case than that in the same vorticity case shown in Fig. 11(b). The reason for a relatively larger core in the case of same vorticity is because there is no dominant centrifugal effect among the two vortices due to the fact that they have the same vorticity, although the size of one vortex is larger than that of the other. The larger core results in a lower frequency of pressure fluctuation in the same vorticity case. In addition, since the eccentricity in the same core size case shown in Fig. 11(a) is larger, it generates higher fluctuation in the source term in Fig. 9 than that in Fig. 10. The above description also demonstrates that dynamic processes such as strengthening of vorticity are able to be captured by the vortex particle method, particularly due to the remeshing process represented by Equation (7), where strengthening or weakening of vorticity is allowed based on spatial re-distributions of vorticity.

4.0 CONCLUSIONS

In a system with multiple vortices without merger, there are identifiable frequencies, each of which can be attributed to either the vorticity in the vortex cores or the motion of the centre of the vortices. When two identical vortices are getting closer to each other, the low frequency related to the rotation motion of the vortex centre becomes higher, and the high frequency related to the core

self-rotation tends to decrease although not significantly. After vortex merger, there is only one frequency resulting from the merged core rotation. In a multiple-vortex-pair system such as those in aircraft wakes, the above-described behaviours do not seem to change in spite of the induction from the mirror image of the vortices with respect to its centreline. In comparing two different two-vortex-pair systems, both with two times of circulation value for the outer vortex pair than that for the inner vortex pair, the system with the same original core size for each of the vortices (thus different vorticity levels) radiates sound with slightly higher magnitude and higher frequency than the system with the same original core vorticity for each of the vortices (thus different core sizes), after the two vortex pairs merge into one vortex pair.

ACKNOWLEDGMENTS

This research was funded under NASA grants NNL04AA77G, and under DOT Volpe contract DTRT57-06-P-80188. The authors would also like to acknowledge the computer hours provided by the SHARCNET of Canada.

REFERENCES

1. ZHENG, Z.C., LI, W., WANG, F.Y. and WASSAF, H. Influence of vortex core on wake vortex sound emission, *J Aircr*, 2007, **44**, (4), pp 1369-1377.
2. HARDIN, J.C. and WANG, F.Y. Sound generation by aircraft wake vortices, December 2003, NASA/CR-2003-212674.
3. ASH, R.L. and ZHENG, Z.C. Numerical simulations of commercial aircraft wakes subjected to airport surface weather conditions, *J Aircr*, 1998, **35**, (1), pp 18-26.
4. HAN, J., LIN, Y., ARYA, S.P. and PROCTOR, F.H. Numerical study of wake vortex decay and descent in homogeneous atmospheric turbulence, *AIAA J*, 2000, **38**, (4), pp 643-656.
5. ZHENG, Z.C. The Betz invariants and generalization of vorticity moment invariants, *AIAA J*, 2001, **39**, (3), pp 431-437.
6. ZHENG, Z.C. and ASH, R.L. A study of aircraft wake vortex behavior near the ground, *AIAA J*, 1996, **34**, (3), pp 580-589.
7. ZHENG, Z.C. and BAEK, K. Inviscid interactions between wake vortices and shear layers, *J Aircr*, 1999, **36**, (2), pp 477-480.
8. ZHENG, Z.C. and LIM, S.H. Validation and operation of a vortex-wake/shear interaction model, *J Aircr*, 2000, **37**, (6), pp 1073-1078.
9. HOWE, M.S. *Theory of Vortex Sound*, 2003, Cambridge University Press, Cambridge, UK.
10. TANG, S.K. and KO, N.W.M. Basic sound generation mechanisms in inviscid vortex interactions at low Mach number, *J Sound and Vibration*, 2003, **262**, pp 87-115.
11. TANG, S.K. and KO, N.W.M. Sound sources in the interactions of two inviscid two-dimensional vortex pairs, *J Fluid Mech*, 2000, **419**, pp 177-201.
12. POZRIKIDIS, C. The nonlinear instability of Hill's vortex, *J Fluid Mechanics*, 1986, **168**, pp 337-367.
13. ZABUSKY, N.J., HUGHES, M.H. and ROBERTS, K.V. Contour dynamics for the Euler equations in two dimensions, *J Computational Physics*, 1979, **30**, pp 96-106.
14. CROW, S.C. Stability theory for a pair of trailing vortices, *AIAA J*, 1970, **8**, pp 2172-2179.
15. CROUCH, J.D. Instability and transient growth for two trailing-vortex pairs, *J Fluid Mech*, 1997, **350**, pp 311-330.
16. MOKRY, M. The vortex merger factor in aircraft wake turbulence, *Aeronaut J*, January 2005, **109**, (1091), pp 13-22.
17. ORLANDI, P. Two-dimensional and three dimensional direct numerical simulation of co-rotating vortices, *Physics of Fluids*, 2007, **19**, pp 013101-1-013101-18.
18. COTTET, G.-H. and KOUMOUTSAKOS, P. *Vortex Methods, Theory and Practice*, 2000, Cambridge University Press.
19. MOHRING, W. On vortex sound at low Mach number, *J Fluid Mech*, 1978, **85**, pp 685-691.
20. MOHRING, W. Modelling low Mach number noise, *Mechanics of Sound Generation in Flow*s, 1979, MULLER, E.-A. (Ed), Springer.
21. KAMBE, T., MINOTA, T. and TAKAOKA, T. Oblique collision of two vortex rings and its acoustic emission, *Physical Review E*, 1993, **48**, pp 1866-1881.
22. KNIO, O.M., COLOREC, L. and JUVE, D. Numerical study of sound emission by 2D regular and chaotic vortex configurations, *J Computational Physics*, 1995, **116**, pp 226-246.
23. MITCHELL, B.E., LELE, S. and MOIN, P. Direct computation of the sound from a compressible co-rotating vortex pair, *J Fluid Mech*, 1995, **285**, pp 181-202.
24. MULLER, B. On sound generation by the Kirchhoff vortex, October 1998, Report No 209/1998, Department of Scientific Computing, Uppsala University.
25. NORBURY, J. A family of steady vortex rings, *J Fluid Mech*, 1973, **57**, pp 417-431.
26. PIERREHUMERT, R.T. A family of steady, translating vortex pairs with distributed vorticity, *J Fluid Mech*, 1980, **99**, pp 129-144.
27. ELDREDGE, J.D. The dynamics and acoustics of two-dimensional leapfrogging vortices, *J Sound and Vibration*, May 2007, **301**, (1-2), pp 74-92.
28. BEALE, J.T. and MAJDA, A. Vortex methods II: high order accuracy in 2 and 3 dimensions, *Math Comput*, 1982, **32**, pp 29-52.
29. ELDREDGE, J.D., COLONIUS, T. and LEONARD, A. A Vortex particle method for two-dimensional compressible flow, *J Comp Physics*, 2002, **179**, pp 371-399.
30. KAO, H.C. Body-vortex interaction, sound generation, and destructive interference, *AIAA J*, 2002, **40**, (4), pp 652-660.
31. ZHENG, Z.C. Far-field acoustic pressure from a system of discrete vortices with time-varying circulation, 2005, AIAA Paper 2005-3005, 11th AIAA/CEAS Aeroacoustics Conference, 23-25 May 2005, Monterey, CA.
32. MELANDER, M.V., ZABUSKY, N.J. and MCWILLIAMS, J.C. Symmetric vortex merger in two dimensions: causes and conditions, *J Fluid Mech*, 1988, **195**, pp 303-340.
33. WAUGH, D.W. The efficiency of symmetric vortex merger, *Physics of Fluids A*, 1992, **4**, (4), pp 1745-1758.
34. SAFFMAN, P.G. and SZETO, R. Equilibrium shapes of a pair of equal uniform vortices, *Physics of Fluids*, 1980, **23**, pp 2339-2342.
35. MEUNIER, P., EHRENSTEIN, U., LEWEKE, T. and ROSSI, M. A merging criterion for two-dimensional co-rotating vortices, *Physics of Fluids*, 2002, **14**, pp 2757-2766.
36. TSUBOI, K. and OSHIMA, Y. Merging of two dimensional vortices by the discrete vortex method, *J Physical Society of Japan*, 1985, **54**, (6), pp 2137-2145.
37. BERTENYI, T. and GRAHAM, W.R. Experimental observations of the merger of co-rotating wake vortices, *J Fluid Mech*, 2007, **586**, pp 397-422.